The evolution of aerosols mixing state derived from a field campaign in Beijing: implications to the particles aging time scale in urban atmosphere

Jieyao Liu[1], Fang Zhang[2], Jingye Ren[3], Lu Chen[4], Anran Zhang[2], Zhe Wang[2], Songjian Zou[2], Honghao Xu[2], Xingyan Yue[1]

[1] School of Geographical Sciences, Hebei Normal University, Shijiazhuang, China

[2] School of Civil and Environmental Engineering, Harbin Institute of Technology (Shenzhen), Shenzhen, China

[3] Xi'an Institute for Innovative Earth Environment Research, Xi'an, China

[4] Faculty of Geographical Science, Beijing Normal University, Beijing, China

Correspondence to: Fang Zhang (zhangfang2021@hit.edu.cn)

Abstract

The mixing states and aging time scale of aerosol particles play a vital role in evaluating their climate effects. Here, ~~we~~by using the field measurement at a site of the urban Beijing, we have identified four different real-time mixing patterns of size-resolved particles ~~using the field measurement by a humidity tandem differential mobility analyzer (H TDMA) in the urban Beijing. We show that the particles with external~~, which are defined as less hygroscopic (LH) internally-mixed, externally-mixed, transitional externally-mixed and ~~internal mixing state during the campaign account for 20 48~~more hygroscopic (MH) internally-mixed particles, with atmospheric fraction of 0-10%, 20-46%, 17-24% and 27-56% respectively ~~and the~~. The fraction ~~highly~~ depends on particles size~~.~~, with the maximum fraction of MH internally-mixed particles at 80 and 110 nm, and the minimum fraction of LH internally-mixed particles across all sizes, implying rapid mixing and aging of ambient

particles during the observational period. The diurnal ~~variation~~variations of the mixing states of particles in all sizes investigated (40, 80, 110, 150 and 200 nm) present an apparent aging process from ~~external~~externally-mixed to ~~internal mixing state,MH~~ internally-mixed, which typically ~~spanning~~spans a duration of approximately 5–~~8~~10 hours from 8:00–10:00 to 15:00–17:00~~.~~, revealing the mixing (aging) timescale of aerosols in polluted urban atmosphere. Additionally, ~~the~~our results ~~illustrate that high ambient temperature during daytime or more humid atmosphere accelerates the aging process of aerosol particles, leading to the particles from external to internal mixing on both clear and cloudy days. Also, with the evolution of particulate pollution, the aerosol particles become more internally mixed. Our result implies~~suggest that those fine aerosol particles experience aging through both the photochemical process and ~~aqueous~~non-photochemical growth ~~in~~during the ~~polluted atmosphere of urban Beijing~~campaign. Furthermore, through a comprehensive review of the mixing/aging timescale of particles adopted in current models and derived from observations, we show the great discrepancy between observations and models, highlighting the importance to parameterize their aging time scale based on more field campaigns.

1 Introduction

The mixing state of atmospheric aerosol particles can affect the hygroscopicity and the ability to serve as cloud condensation nuclei (CCN), and thus the air quality and climate (Müller et al., 2017; Xu et al., 2021; Yao et al., 2022; Ge et al., 2024). It has been shown that the aerosol mixing state is closely related to the hygroscopicity (Chen et al., 2022; Fan et al., 2020). Ren et al. (2018) predicted the concentration of CCN using five different mixing state schemes and found that the influence of aerosol mixing state on its activation characteristics ranged from –34% to +16%. Neglecting particle mixing structure can also lead to significant overestimation of the aerosol absorption efficiency (Yao et al., 2022). Therefore, it is

51 important to account for the information of mixing state of ambient particles in climate

52 models so as to reduce the uncertainty in evaluating their environmental and climate effects.

53 The mixing states of ambient particles are complex. Particles in areas affected by

54 primary emissions are mainly with external mixing state (i.e., the chemical components of

55 particles exist independently), while aerosols in relatively clean areas are mainly transported

56 from elsewhere and have a higher degree of internal mixing (Swietlicki et al., 2008; Enroth et

57 al., 2018; Chen et al., 2022). Internal mixing typically includes uniform composition or core–

58 shell structures (Jacobson et al., 2001). The former refers to the same proportion of species in

59 any part of the aerosol component, while the latter is defined as the mixing state formed by

60 certain chemical components coating or condensing on the surface of other components

61 during the aging process. Also, the mixing state of aerosol particles is variable. Freshly

62 emitted particles undergo various processes, including photochemical and aqueous-phase

63 processes, as well as physical processes such as coagulation and condensation, leading to an

64 increase in their degree of internal mixing. This gradual transition from external to internal

65 mixing characterizes the aging process of particles. The aging timescale varies greatly

66 between clean and polluted areas (Peng et al., 2016; Chen et al., 2017; Ghosh et al., 2021).

67 However, the timescale of aging process of particles was commonly fixed in many models

68 and did not depend on environmental conditions (Chen et al., 2017; Ghosh et al., 2021),

69 which may introduce great uncertainty in the prediction of regional aerosol concentration and

70 the evaluation of aerosol climate effects (Ghosh et al., 2021). Therefore, capturing the

71 temporal scales of the evolution of the aerosol mixing state based on field campaigns is

72 crucial for accurately parameterizing the aging timescale of aerosol particles in models,

73   thereby enhancing the precision of simulations pertaining to the environmental and climatic

74   impacts of aerosols.

75   At present, some studies have characterized the mixing state and aging process of black

76   carbon (BC) aerosols using different instruments. Transmission electron microscopy (TEM)

77   has been used to determine the mixing state of individual particles in China (Li et al., 2016;

78   Zhang ~~J.~~ et al., 2023). However, based on TEM technique, a large number of aerosol samples

79   are required so as to make the results with the significance of statistics, which means a high

80   cost both on labors and materials. The most important issue is that the mixing state of

81   particles may change during collection and transportation. Recently, aerosol time-of-flight

82   mass spectrometry (ATOFMAS) and soot-particle aerosol mass spectrometry (SP-AMS) have

83   been used to measure the mixing state of BC and coated aerosol species in real time (Liu et

84   al., 2019; Xie et al., 2020). Overall, previous studies focused more on the mixing state of BC

85   of single-particles (Saha et al., 2018; Xie et al., 2020; Chen et al., 2020). While, the mixing

86   state of particles across a population in ambient atmosphere is more complex (Riemer et al.,

87   2019). ~~For example, aerosols containing two or more components may also exhibit external~~

88   ~~mixing, as evidenced by the bi- or trimodal distributions~~According to Winkler's definition,

89   the "internal mixing" means when all particles within the bulk aerosol populations are with

90   the same compositions. While, the "external mixing" means when all particles consist of pure

91   species and have distinct compositions (Winkler et al., 1973; Riemer et al., 2019). Note that

92   in Riemer et al. (2019), the definition refers to the bulk not the sized-resolved mixing state of

93   aerosol particles. In this study, the size resolved mixing state of aerosol particles has been

94   identified according to the patterns of the probability density function of hygroscopic growth

factor/hygroscopic parameter (κ) (Gf-PDF; κ-PDF) measured using a humidity tandem differential mobility analyzer (H-TDMA) (~~Fan et al., 2020; Chen et al., 2022; Zhang S. et al., 2023). The mixing state of particles has been retrieved according to the patterns of Gf-PDF/κ-PDF~~ (Hong et al., 2018; Shi et al., 2022; Spitieri et al., 2023). For example, the internally-mixed aerosol populations with diameter of 40 nm are characterized by the single hygroscopic mode of Gf-PDF/κ-PDF, while the externally-mixed particles have bi- or trimodal distributions of Gf-PDF/κ-PDF. However, most studies based on the H-TDMA measurements only made qualitative descriptions of the particle mixing state when explaining the variations in the aerosol hygroscopicity (Wang et al., 2019; Chen et al., 2022; Shi et al., 2022).

In this study, with the aim of obtaining insights into the mixing state and mixing (aging) time scale of ambient particles in urban area, we have identified four different types of size-resolved particles mixing states, and characterized their real-time variations using the field measured hygroscopic growth factor by the H-TDMA in urban Beijing. ~~The dependence of mixing state of particles on temperature (T), relative humidity (RH) and the pollution levels was investigated.~~ The evolution of mixing state of particles with specific sizes was ~~also~~ explored to imply the mixing (aging) timescale of their aging from the diurnal variations during clear and cloudy days. Finally, we compared the mixing/aging timescale of aerosol particles with that adopted in current models and other field observations reported in previous literatures.

2 Methods

The campaign was conducted at the meteorological tower branch of the Institute of Atmospheric Physics (IAP), Chinese Academy of Sciences to measure the physical and

chemical properties of particles and the meteorological conditions from 19 May to 18 June 2017 in Beijing. The instruments used in this study were deployed in a container at ground (the sampling inlet is located at ~8 m on the meteorological tower). The hygroscopicity of aerosols with different dry sizes (40, 80, 110, 150 and 200 nm) and particle number distribution in the size range of 10–550 nm was measured using a H-TDMA and a Scanning Mobility Particle Sizer (SMPS), respectively. The mass concentration of the non-refractory chemical compositions in particulate matter with diameter < 1 μm (PM_1) was measured by an Aerodyne high-resolution time-of-flight aerosol mass spectrometer (HR-ToF-AMS) (Xu et al., 2019), and the BC was measured by a 7-wavelength aethalometer (AE33, Magee Scientific Corp). More details about the sites, instruments and calibrations can be found in previous literatures (Zhang et al., 2017; Wang et al., 2019; Fan et al., 2020; Chen et al., 2022). Since the campaign site was located at the urban area of Beijing, where the atmospheric fine aerosols are more frequently affected by local traffic and cooking sources (Sun et al., 2015). In addition, during the observation period of summertime, the site was predominately affected by the warm and humid southeastern air parcels (Figure S1); while the dust events normally originate from northwestern regions occurring in springtime (Li et al., 2020) and typically with particle sizes in coarse mode (Wang et al., 2023). to measure the Gf of particles with different dry sizes (40, 80, 110, 150 and 200 nm) using a H-TDMA from 19 May to 18 June 2017 in Beijing. The instrument used in this study has been described previously (Zhang et al.,Therefore, the contribution from dust aerosols could be negligible in this study. 2017; Wang et al., 2019; Fan et al., 2020; Chen et al., 2022). Here, we mainly describe the interpretation criteria for the mixing state of particles. The Gf-PDF was obtained by $TDMA_{inv}$ algorithm in this study (Gysel et al., 2009). Then, the κ-PDF of size-resolved particles was retrieved according to the κ-Köhler theory (Petters and Kreidenweis, 2007). Subsequently, we accurately defined four mixing states based on the κ-PDF patterns and the

number of peaks in κ-PDF (Figure 1, Figure ~~S1). Given that the freshly emitted hydrophobic~~ ~~particles showed an external mixing state (Li et al., 2016), the κ-PDF, that exhibited only one~~ ~~nearly~~ S2). The κ-PDF of type 1 exhibits bimodal distributions with a much higher proportion (> 70%) of hydrophobic mode or less hygroscopic mode (LH; the peak of κ-PDF occurs at κ < 0.1~~) mode,~~), was thus defined as LH ~~external mixing~~internally-mixed state (type 1). Mixing type 2 ~~indicates~~refers to that the ~~maximum peak of κ-PDF occurs at~~exhibits bimodal distributions in both LH ~~mode or~~and more hygroscopic (MH, ~~the peak of κ-PDF occurs at~~ ~~$\kappa \geq$~~$\kappa \geq$ 0.1) ~~mode, and the bimodal distributions of the LH and MH~~ modes ~~are present in κ-PDF. Moreover, the~~, with the difference of less than 30% between the fraction of the two modes. The κ-PDF pattern with trimodal distributions ~~called~~was named as transitional ~~external mixing~~externally-mixed state ~~in this study~~ (type 3). The κ-PDF of type 4 was dominated by MH mode, ~~displaying nearly unimodal patterns,~~normally with a fraction of lager than 70%, was defined as ~~internal mixing type~~MH internally-mixed type. It should be noted that the four categories defined in our study have covered all cases of the observational results. In this study, we also calculated the standard deviation of κ-PDF (σ) according to Spitieri et al. (2023), which indicates the degree of dispersion in the data, and is thought to reflect the mixing degree of particles to a certain extent. Given that the aerosol particles sampled at the campaign site in this study are rarely affected by other hygroscopic aerosols (e.g., aerosols from marine sources), the MH internally-mixed particles (110, 150 and 200 nm) are thus mainly from the aging and growth of smaller particles. In contrast, the larger LH internally-mixed particles are predominantly from primary emissions. Therefore, the proportion of MH and LH internally-mixed particles at 100-200 nm can be used to distinguish the contribution to the internally-mixed fraction of larger particles from smaller aerosol aging and primary emissions respectively. Specifically, the result shows that a significant proportion of the internally-mixed particles at larger size originate from the aging

168 and growth of smaller particles, accounting for 99%, 96% and 92% respectively for 110, 150

169 and 200 nm particles, whereas the contribution from primary emissions to these larger

170 internally-mixed particles is less than 10%.
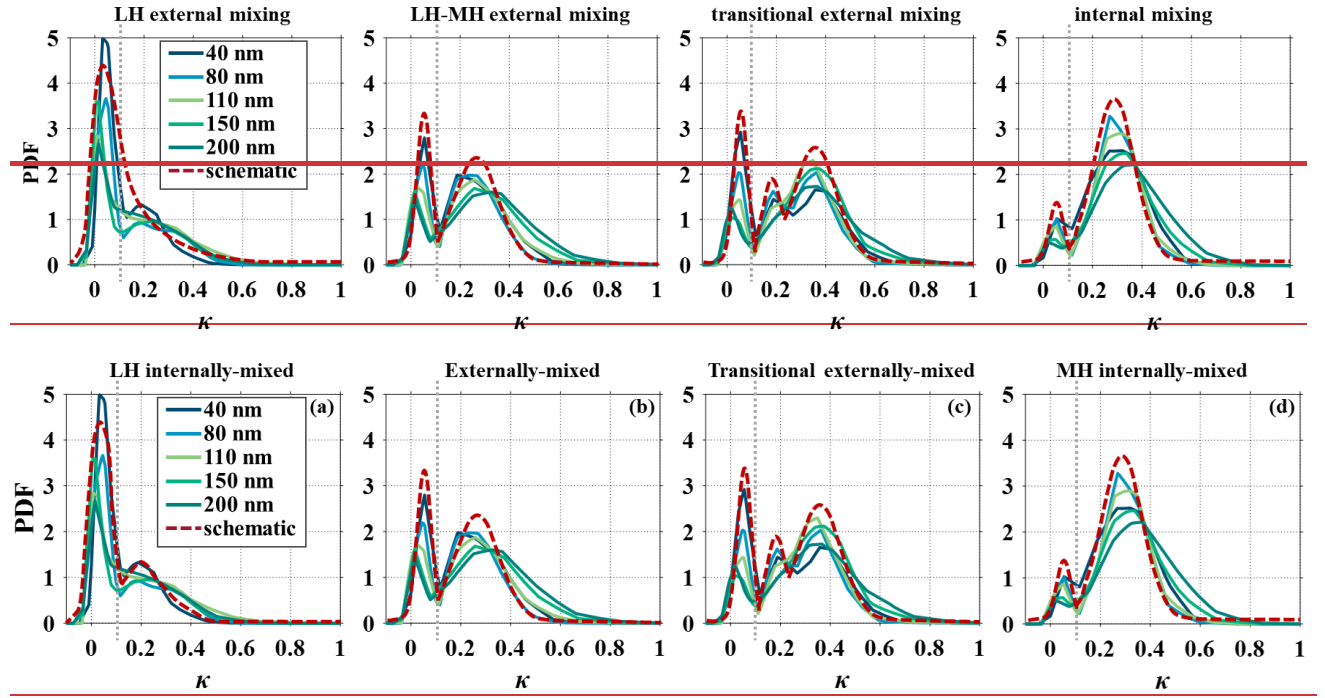
173 Figure 1. The mean κ-PDF of five particle sizes and the schematic diagram of κ-PDF for

174 four mixing types.

3 Results and discussion

3.1 Overview of the mixing state of size-resolved particles

177 Figure 2 shows the time series of size-resolved κ, and κ versus σ. The real-time changes

178 in the mixing states of particles are represented by different filled colors. The κ shows large

179 variationsvalues vary from 0 to 0.5 in each of the five particle sizes, ranging from 0 to 0.5,

180 accompanied by significant changes in mixing states. In general, the mixing state of particles

181 gradually transitions from external mixingexternally-mixed to internal mixingMH internally-

182 mixed along with increases in κ. For example, particles with size of 40 nm are dominated by

183 LH external mixinginternally-mixed and LH-MH external mixing statesexternally-mixed at κ

184 < 0.2; and the transitional external mixingexternally-mixed state take up an increasingly

185 proportion often corresponding to κ values of >~~ ~~0.2 and the ~~internal mixing state occurs~~MH

186 internally-mixed particles occur when κ greater than 0.3 (shown by the light gray dots in

187 Figure 2).

188 However, there exists different correlations between κ and σ for the five sizes. For

189 particles ~~smaller than 100 nm (i.e.,~~ with diameter of 40 and 80 nm~~),,~~ the σ increases as the κ

190 increases from 0.1 to 0.4 along with slight increase in the fraction of MH internally-mixed

191 particles, showing a positive correlation. While, unlike the small particles, the σ for particles

192 larger than 100 nm (i.e., 110, 150 and 200 nm) exhibits a negative ~~trend~~correlation to κ

193 variations, ~~with~~showing that the ~~internal mixing and strong~~ particles were more MH

194 internally-mixed and with stronger hygroscopicity ~~but the smaller the value of σ. Our result~~

195 ~~contrasts with that previously observed in a vegetated site by Spitieri et al. (2023), which~~

196 ~~used only σ of Gf-PDF as a single indicator to characterize~~when the ~~particles mixing state.~~

197 ~~Our result indicates that the parameter σ alone cannot characterize the mixing state~~smaller σ

198 values were derived. The different sources and chemical compositions of ~~particles in~~

199 ~~megacity of Beijing, where the~~ aerosol particles ~~are usually severely affected by~~could explain

200 the distinct relationship between σ, mixing states and hygroscopicity among particles of

201 different sizes. Here, the standard deviation of κ-PDF, σ, reflects the degree of dispersion in

202 the pattern of κ-PDF. Taking 40 nm particles as an example, the obtained larger σ value

203 indicates more diversity in particles hygroscopicity and chemical compositions, and thus a

204 higher degree of external mixing state. This is because that, besides the local ~~anthropogenic~~

205 emissions (Ren et al., 2023), the 40 nm particles during the campaign were also from the

206 growth of newly formed particles which are much more hygroscopic (Liu et al., 2021a).

207 Therefore, the composition of those small particles is more heterogeneous, resulting in both

208 greater σ and κ. The cases where both the σ and κ of small particles are lower suggest that the

209 particles may consist of a mixture of different species originating from primary emissions

210   (e.g., BC, hydrocarbon-like and/or cooking organic aerosols). While, for most of larger

211   particles, their chemical composition tends to become homogeneous after aging and growth

212   processes, exhibiting stronger hygroscopicity, a higher degree of internal mixing, and thus the

213   smaller σ. However, a small number of larger particles with weak hygroscopic properties

214   from primary emissions coexist with the aged ones in the atmosphere, which would result in

215   larger σ and higher degree of external mixing.

216
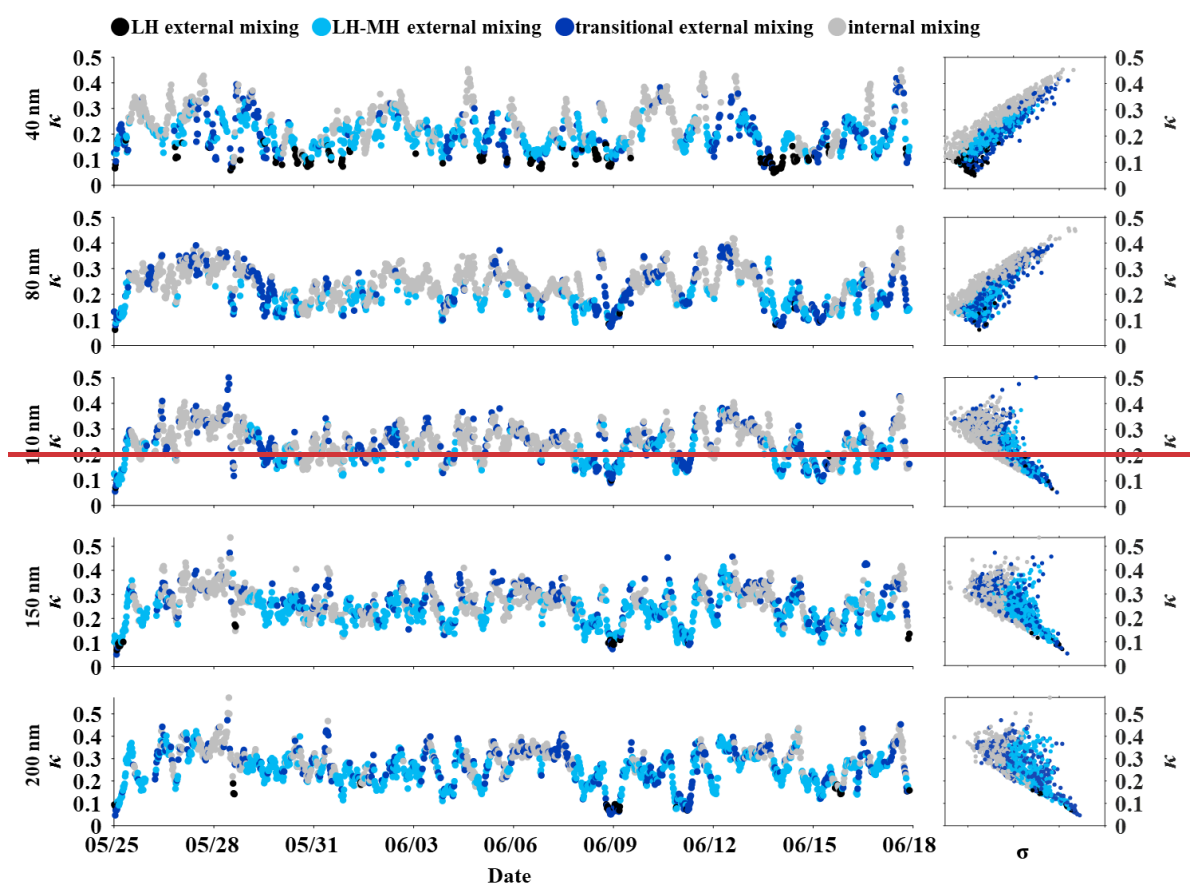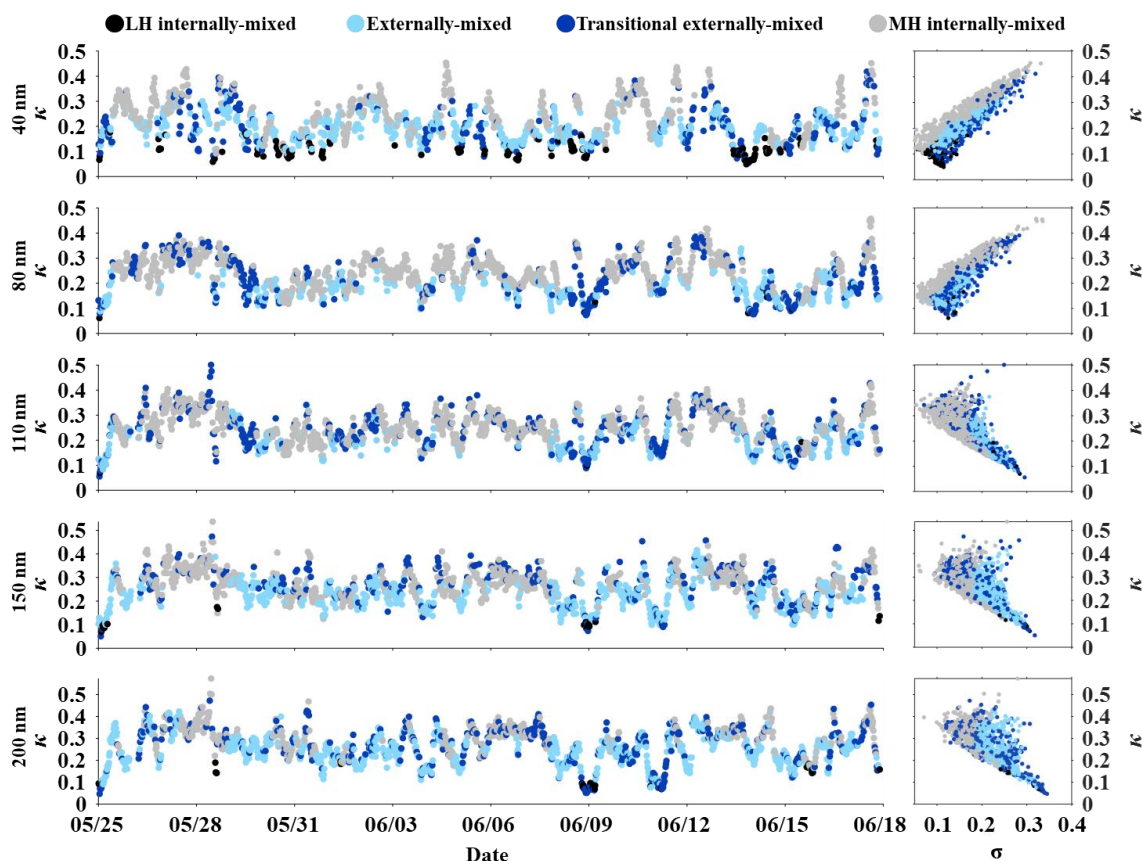
Figure 2. Time series of hygroscopic parameter (κ), and plots of κ versus standard deviation

of κ-PDF (σ) for 40, 80, 110, 150 and 200 nm particles (from top to bottom). The colors

denote the different mixing types.

The size dependence of mixing type fractions and σ are shown in Figure 3. The external

mixing types, including ~~LH external mixing state~~externally-mixed and ~~LH MH external~~

~~mixing state~~transitional externally-mixed states, dominate in 40, 150 and 200 nm particles,

accounting for ~~47%, 41~~53%, 57% and ~~48~~70% respectively of all mixing types. The elevated

fraction ~~in~~of externally-mixed particles ~~with external mixing state~~ is intimately associated

with the local sources. For instance, a previous study revealed the particle size distribution of

aerosols from different sources in urban Beijing, suggesting that the particles with ~~40~~

~~nm~~diameter of 40 nm during rush hours and cooking times predominantly originated from

229 primary emissions, and particles ~~with~~at 150 and 200 nm displayed a strong correlation with

230 ~~transportation sources and biomass burning~~regional atmospheric transport sources (Ren et al.,

231 2023). In this study, the particles exhibit weaker hygroscopicity at lower wind speeds,

232 indicating that hydrophobic particles are primarily from local sources (Figure S3).

233 Furthermore, for 40 nm particles, ~~besides the impact from primary sources,~~ the

234 ~~relative~~relatively higher fraction of MH internally-mixed particles ~~with internal mixing state~~

235 (37%) is likely due to ~~that~~ the growth and aging ~~process~~ of newly ~~generated~~formed particles

236 ~~that are with high hygroscopicity (Wu et al., 2016;~~ (Liu et al., 2021a). This is similar to the

237 result observed in Athens, Greece, in which the particles with 30 nm were more internally-

238 mixed (Spitieri et al., 2023). While, for particles with sizes of 80 and 110 nm, the transitional

239 ~~and internal mixing~~externally-mixed and MH internally-mixed states totally account for 50-

240 80% of all mixing types, corresponding to a significant decrease from about 10% to less than

241 1% of the fraction of the LH ~~external mixing~~internally-mixed type. Note that the proportion

242 of transitional ~~external mixing state remains~~externally-mixed particles remain relative

243 constant, with a mean value of 21% across all sizes in this study, implying a continuous

244 influence of atmospheric aging process on the particles mixing state. In addition, the 80 and

245 110 nm aerosols may continue aging and form 150 and 200 nm aerosol particles. Therefore,

246 the aging of this group of aerosols should be more advanced, showing that the fraction of

247 internally-mixed particles at 80 and 110 nm was the highest among the five particle sizes. On

248 average, the result reveals that the externally and internally mixed particles accounted for

249 ~~56%±12~~53%±11% and ~~44%±12~~47%±11% respectively. The mixing state of particles derived

250 in this study differs from that reported by Zhang et al~~.,~~. (2017), in which they conducted the

251 measurements at a suburban site of Xinzhou, where the aerosols ~~is~~are much less affected by

252 sources nearby, and the aerosols are mainly transported from elsewhere and are thus more

253 aged and well mixed. The result implies that the influence of mixing state on hygroscopicity

254 should be explored at specific particle sizes due to the heterogeneity of chemical

255 compositions with particle size (Fan et al., 2020, Figure ~~S2~~S4).

256

257
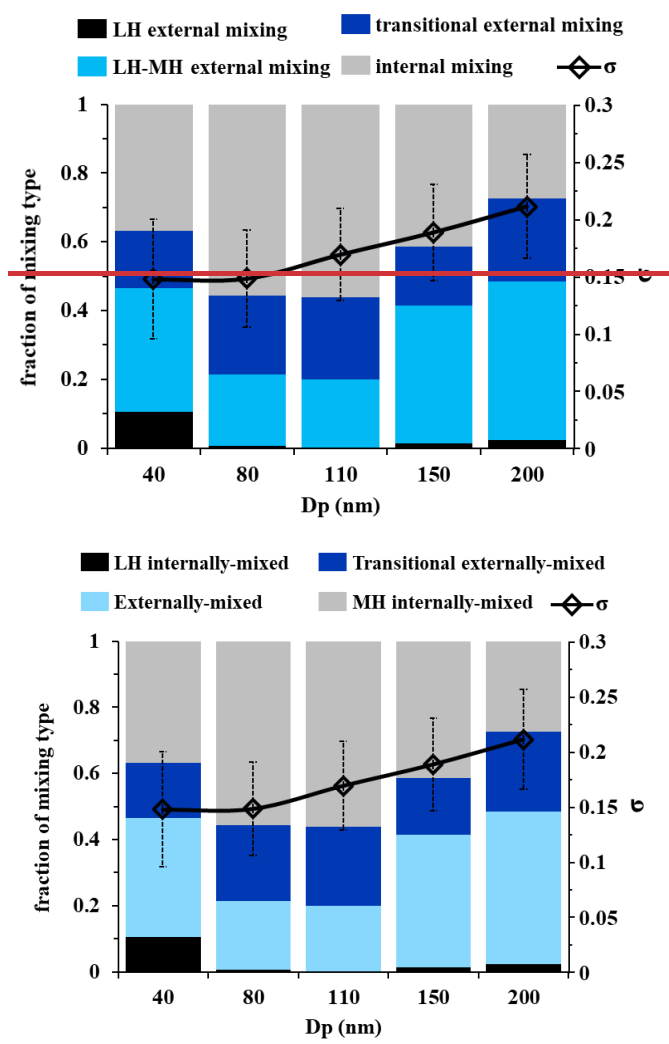
258 Figure 3. The size dependence of fraction of particles mixing types and σ.

259   Further, we compared the dependence of κ and σ on the variations of mixing states for

260 five particle sizes (Figure 4). At 40 and 80 nm sizes, it shows that both κ and σ increases

261 markedly when the particles change from ~~external to internal mixing state.~~externally-mixed

262 to MH internally-mixed. While, for particles with sizes of 110, 150 and 200 nm, the σ

263 reduced but the κ increased when the particles change from ~~external~~externally to ~~internal~~

264 ~~mixing~~internally-mixed state. In other words, the σ of the particles larger than 80 nm shifts to

265 lower values as the particles become more internally mixed. ~~Our results indicate that the~~

266 ~~standard deviation of κ-PDF alone is insufficient to characterize mixing degree in polluted~~

267 ~~area.~~ This contrasts with that previously observed in a vegetated site by Spitieri et al. (2023),

268 which used only σ of Gf-PDF as a single indicator to characterize the particles mixing state.

269 The distinct relationship between mixing type and σ for small particles (i.e., 40 and 80 nm) in

270 urban sites indicates that the standard deviation of κ-PDF can effectively characterize mixing

271 degree and chemical composition heterogeneity of larger particles in polluted area, where

272 smaller aerosol particles are usually severely affected by local anthropogenic emissions.

273
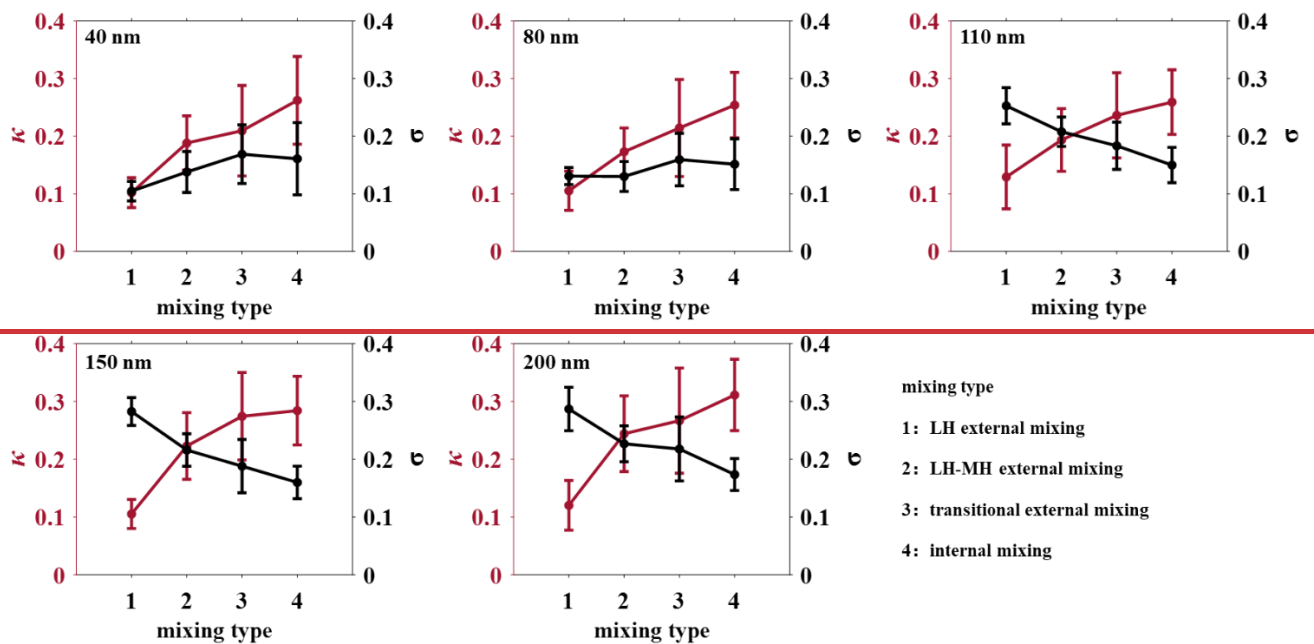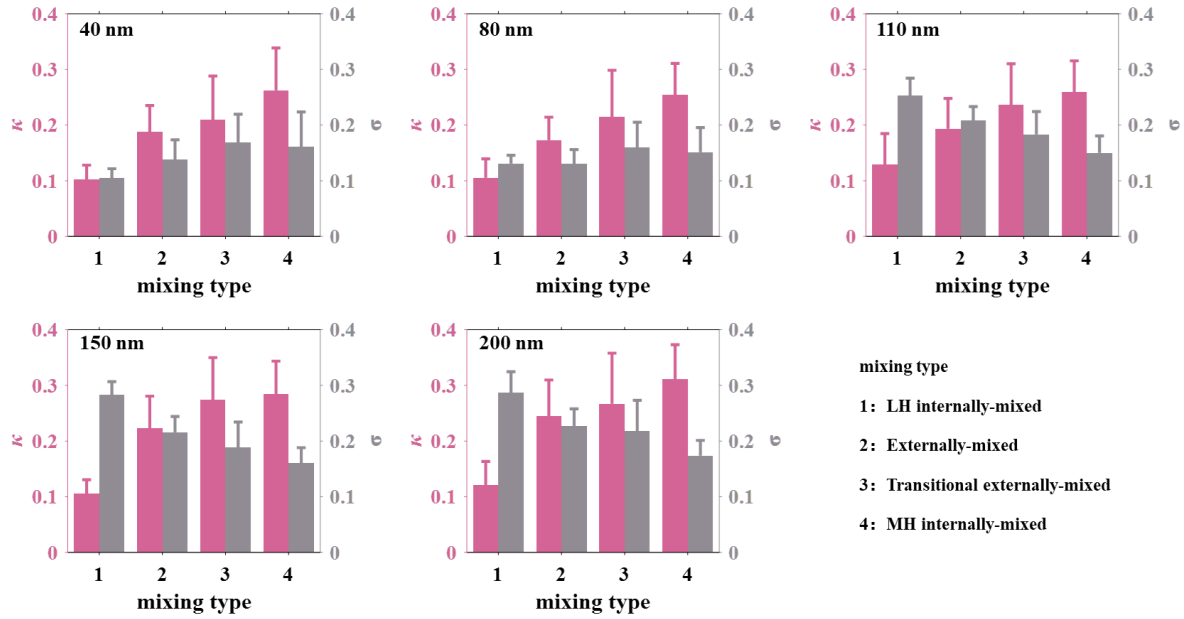
Figure 4. The mixing type dependence of hygroscopicity and σ for five particle sizes.

3.2 Evolution of mixing state of the particles

~~3.2.1 Diurnal variations~~

The average diurnal variations of the mixing state and κ of different particle sizes are shown in Figure 5. For 40 nm particles, the fraction of LH ~~external mixing state~~internally-mixed particles presents three peaks at morning (9:00–12:00 local time; LT), evening rush hours (18:00–20:00 LT) and nighttime (0:00–03:00 LT). This is accompanied with the impacts from those primary cooking and traffic emissions (Xu et al., 2021; Liu et al., 2021b). Unlike the 40 nm particles, there is no apparent increase of ~~external mixing~~externally-mixed state for the particles with sizes of 80, 110, 150, and 200 nm in the rush hours or cooking times. The results indicate that the particles emitted from local primary sources are small mainly with sizes around 40 nm during the campaign. Correspondingly, the proportion of the particles with ~~internal mixing~~MH internally-mixed state was smallest in the morning and nighttime, but exhibiting a rapid increase from about 9:00 until the evening rush hours (about 16:00–18:00). ~~The particles with LH MH external mixing and transitional external mixing state represent the intermediate state of the aging process in which particles transition from~~

291 ~~external mixing to internal mixing~~This is accompanied by the increase of hydrophobic modes

292 in κ-PDFs of small particle sizes during rush and cooking hours measured in Beijing (Figure

293 S5). Moreover, the increase of externally-mixed particles of 40 nm at nighttime may be

294 highly associated with the emissions of primary species from heavy trucks in urban Beijing at

295 nighttime (Hua et al., 2018), which can also be evidenced by the increased hydrophobic mode

296 of the 150 nm and 200 nm particles observed from 00:00 to around 3:00 in Figure S5. In

297 addition, the absence of photochemical aging and the lower boundary layer height during

298 nighttime could also result in a higher proportion of externally-mixed particles. In addition,

299 the externally-mixed and transitional externally-mixed particles represent the intermediate

300 state of the aging process in which particles transition from LH to MH mode, and both

301 showed a decrease to around 10% during the corresponding period of the day as the

302 proportion of particles with ~~internal mixing state increased up to 80%. The diurnal variations~~

303 ~~imply an apparent aging process that leads the particles changed from external mixing in the~~

304 ~~early morning to internal mixing in the afternoon. The aging process also changes particles~~

305 ~~physiochemical properties.~~MH internally-mixed state increased up to 80%. As a result, an

306 obvious enhancement in particles hygroscopicity was observed during the daytime, indicating

307 the impact of particles mixing and aging on their hygroscopicity (Hersey et al., 2013; Müller

308 et al., 2017). Overall, the diurnal variation implies an apparent aging process that leads the

309 particles changed from externally-mixed in the early morning to MH internally-mixed in the

310 afternoon.
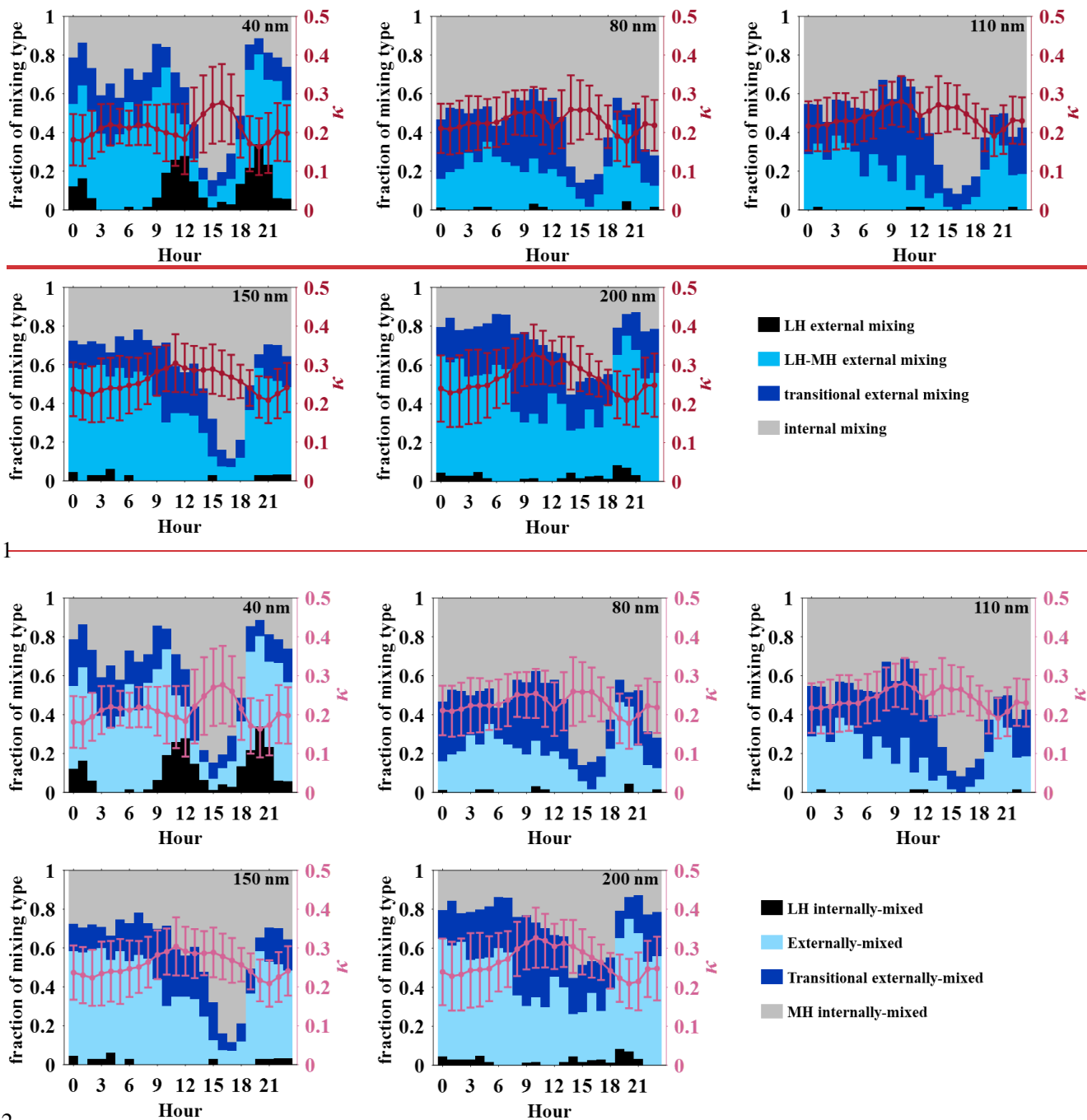
Figure 5. Diurnal variations of the mixing state fraction and κ for five particle sizes.

dependence of mixing state of the particles across all observed sizes on T, for example, for the 40 nm particles, the fraction with external mixing state reduces from 60% to 20%, while that of the internal mixing state increases from 30% to 70% with the increase of T from <20°C to >35°C. This can be easily explained that the higher ambient T (usually corresponding to the periods in daytime) will generally promote the photochemical aging and mixing of the particles (Riemer et al., 2004; Zhang et al., 2015). But note that, the fraction of particles with internal mixing state decreases evidently when the T increases from 15 °C to about 25°C. With the increase of RH from 20% to 80%, the fraction of particles with internal mixing state at 40 nm reduces from 60% to 20%. However, the fraction of the internal mixing state for particles larger than 80 nm is reduced with the increase of RH when its value <60%, while it increases with the RH increase as it larger than 60%, indicating that the very humid atmosphere with high RH is more favorable for particle aging that was reported promoted by the aerosols aqueous process (Zhang et al., 2021).

With the evolution of PM$_1$ pollution, the fraction of internal mixing state for 40 nm particles significantly decreases to less than 10% due to accumulation of small particles from local primary emissions under heavy pollution conditions, which thus leads to enhanced heterogeneity of particles chemical composition and externally mixed degree (Fan et al., 2020). While for particles with sizes of 80, 110, 150 and 200 nm, the proportion of internally mixed state increase to nearly 90% under heavy PM$_1$ pollution, which is consistent with previous observations in winter of urban Beijing (Chen et al., 2020) and in Xi'an (Wang et al., 2014). Our result implies that those fine aerosol particles experience aging through both the photochemical processes and aqueous growth in the polluted atmosphere of urban Beijing,

340 ~~thereby affecting their mixing state.~~

341
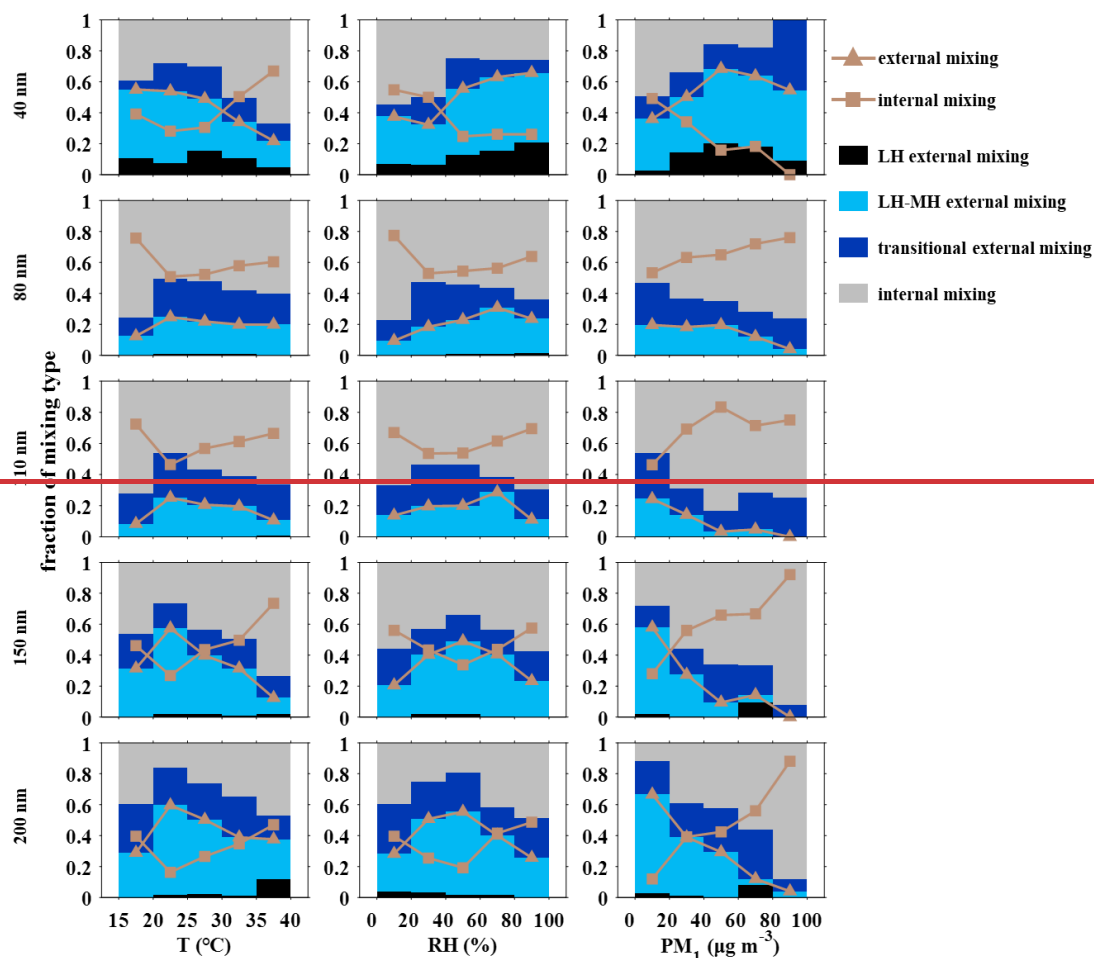
342 ~~Figure 6. Mixing type fraction as a function of T, RH and PM₁ for five particle sizes. Solid~~

343 ~~triangles and solid squares represent the fraction of internal and external (LH external mixing~~

344 ~~+ LH-MH external mixing state) mixing states, respectively.~~

345 **3.3 Particles mixing (aging) timescale: on clear and cloudy days**

346 ~~Figure 7 shows the average~~The aerosol particles mixing and aging process is usually

347 accompanied by the growth of particle sizes. In order to derive the mixing and aging

348 timescale of particles, we further analyzed the averaged diurnal variations of ~~the fraction of~~

349 particles fraction with ~~internal mixing~~MH internally-mixed state, particle number size

350 distributions (PNSD) and the variations of mean ~~fractions of all~~κ-PDF during the ~~four mixing~~

351 ~~types~~growth periods on both clear and cloudy days. (Figure 6). On clear days, the fraction of

~~internal mixing state~~MH internally-mixed particles increases significantly from ~10-40% before 9:00 to nearly 100% during 12:00–15:00, especially ~~when particle size smaller~~for particles larger than ~~150~~40 nm. ~~While, there is no such notable~~Such enhancement is nearly as large as that on cloudy days. ~~The difference in~~In detail, the proportion of MH internally-mixed particles ~~with internal mixing state~~usually increased by less than 50% between the period before 9:00 and during 12:00–17:00 ~~usually does not exceed 50% on cloudy days~~, and ~~the~~its maximum ~~fractions of particles with internal mixing state on cloudy days were about~~fraction was around 50%-90%. ~~Compared with the cloudy days~~While, the fraction of MH internally-mixed particles ~~with internal mixing~~ for 40 nm is noticeably higher on clear days~~, which accounts for about 40% of all mixing states, indicating that the 40 nm particles are likely from nucleation processes. On clear days,~~ (80%), which is approximately 40% greater than that on cloudy days, indicating that photochemical processes can make particles more internally-mixed and aged (Liu et al., 2021a). Furthermore, the diurnal variations of PNSD show that the growth of particle size is highly consistent with the increase of the fraction of MH internally-mixed particles. Additionally, the particles κ with large sizes at the corresponding times in the PNSD also shows an increase on both clear and cloudy days. Specifically, as the particle size grows from less than 40 nm before 9:00 to ~100 nm around 17:00, the fraction of MH internally-mixed particles increases from less than 40% to >90%. And, the peak value for κ shifts from $\kappa < 0.1$ to $\kappa > 0.2$, and the count for the peak value of κ-PDF increases accordingly (Figure 6). Overall, on clear days, the particles undergo a gradual shift from ~~external to internal mixing~~externally-mixed to MH internally-mixed states during 8:00–16:00 accompanied by a growth in particle size from 20 nm to about 100 nm ~~(Figure S3),~~, which is generally 1–2 hours shorter than that observed on cloudy days.

~~Overall, the~~The obvious banana-shape growth of newly formed particles was captured in the diurnal variations of PNSD, which characterizes that the aging and growth of non-

377 hygroscopic particles (e.g., BC) of primary emission and newly generated particles. Overall,

378 the mixing and aging process is confirmed by the transition of particle from

379 ~~external~~externally-mixed to ~~internal mixing states,~~MH internally-mixed, as well as the

380 growth of particle size, ~~and the increase of secondary organic aerosol (Figure S3),~~ which

381 typically spans a duration of approximately 5 to ~~8~~10 hours, as is similar to the aging

382 timescale of aerosol particles in the polluted Indo-Gangetic Plain (< 10 hours) (Ghosh et al.,

383 2021). Actually, the aerosol particles aging would be largely affected by local atmospheric

384 conditions, and thus would vary both spatially and temporally (Pöschl et al., 2001; Huang et

385 al., 2013). For example, using an environmental chamber approach, Peng et al. (2016)

386 revealed that the timescale of BC aerosols aging is 2.3 and 4.6 hours, 9 and 18 hours over two

387 cities—Beijing and Houston respectively. Note that the faster aging time in Beijing derived in

388 the chamber experiment is probably due to the different levels in the concentration of gaseous

389 precursors. In addition, there is only photochemical aging occurred in the chamber

390 experiment, however, in the atmosphere, the particles aging is also through coagulation

391 process which usually occurs slower than the photochemical reaction and condensation

392 processes (Chen et al., 2017). This can also explain our observed faster mixing (aging) time

393 on clear days when the photochemical process is more significant considering that the

394 difference of the pollutant concentrations in daytime between clear and cloudy days is not

395 obvious (i.e., ~~SO_2, NO_2, O_3,~~O_X and PM_1; Figure ~~S4~~S6).

396
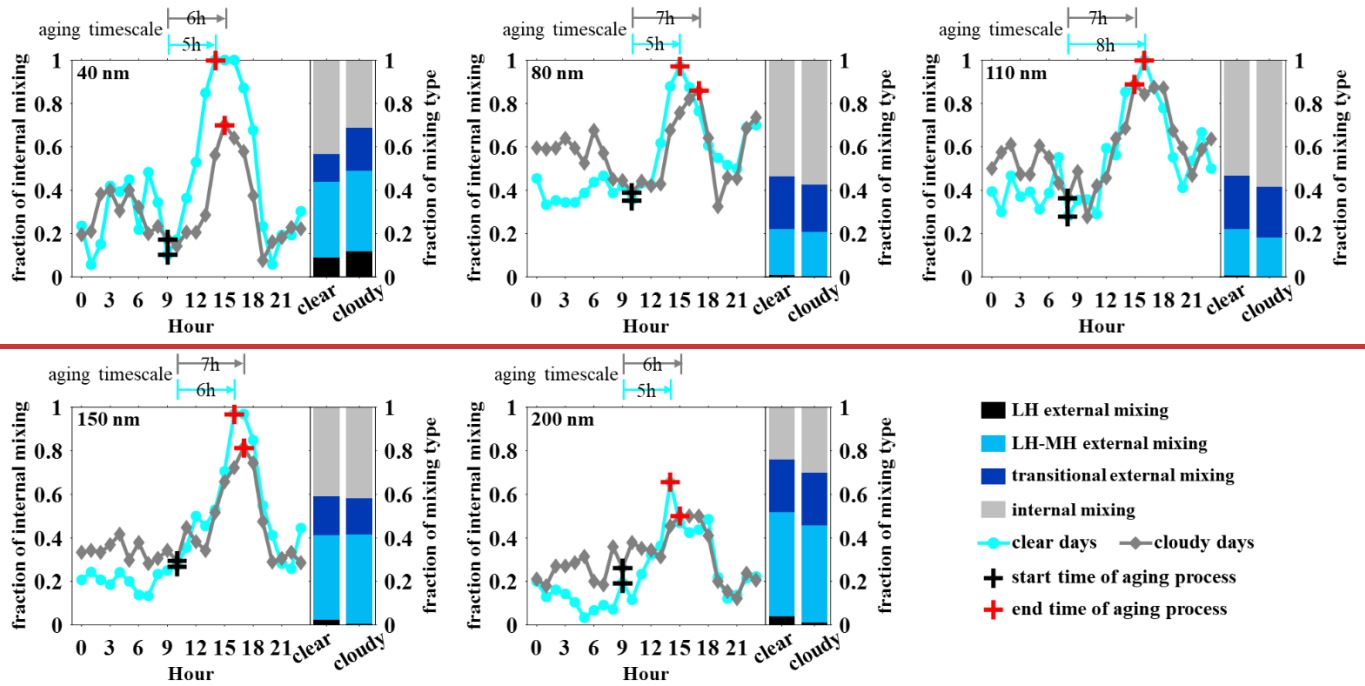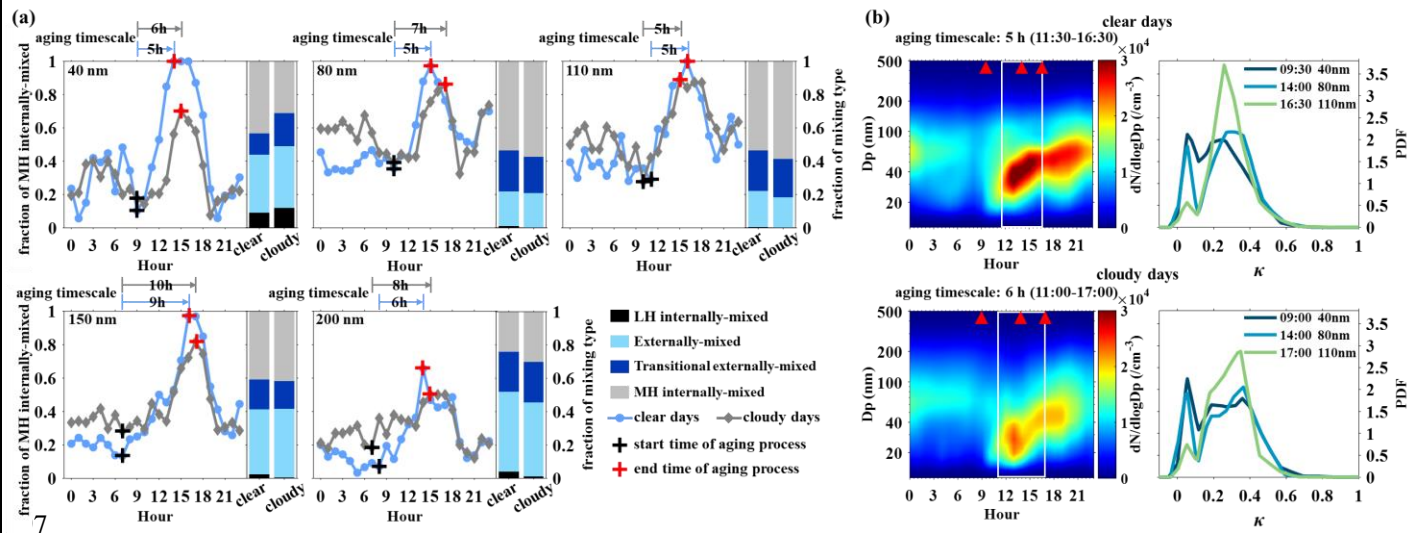
Figure 7.6. (a) Diurnal variations of ~~internal mixing~~the proportion of MH internally-mixed

particles and statistical results of the fraction of mixing state for five particle sizes on clear

and cloudy days. ~~The line segments and time above the graph represent the aging timescale of~~

~~particles. The~~ The start time ~~and end time~~ of particle mixing/aging ~~process~~ was selected when

the proportion of MH internally-mixed particles ~~with internal mixing state~~ is ~~closest~~

~~after~~minimum between sunrise~~, and~~ and noon, and the end time was defined as when the

fraction of MH internally-mixed particles reaches its maximum~~, represented by black~~. (b) The

averaged diurnal variations in PNSD and the variations of mean κ-PDF during the growth

periods on clear and cloudy days (right panels). The red crosstriangles indicate 2 hours before

the start of the aging, during the growth and end of the aging process respectively.

3.4 Implications to parameterization of the current models

The mixing/aging timescale of aerosol particles significantly impacts their

physiochemical properties, which in turn affects their atmospheric lifetime, transport

characteristics (Zhang J. et al., 2023)), hygroscopicity and the direct radiative forcing of

aerosol particles (Moffet and Prather, 2009; Wang et al., 2018; Stevens and Dastoor, 2019).

We further compared our results with the results derived from five field sites and the values

adopted in current models (Table S1). In most models, the aging processes of carbonaceous

aerosols were treated with a simple parameterization, which generally obtained aging time

based on the transformation of aerosols from hydrophobic to hydrophilic (Chen et al., 2017;

Ghosh et al., 2021). As shown in Figure 8, the aging timescale of particles in Beijing

achieved in this study is 5-8 hours, which is comparable with the observations of that

reported in other urban areas likeUnlike the models, the aging timescale of BC aerosols in

field measurements and laboratory studies was commonly derived by tracking changes in

hygroscopicity, morphology, coating thickness or optical properties (Moffet and Prather, 2009;

Akagi et al., 2012; Krasowsky et al., 2016; Peng et al., 2016). These methods were used to

quantify the aging timescale of particles indirectly. While, in our study, the mixing (aging)

time was inferred based on the changes in hygroscopic modes and mixing states of non-BC

particles in the ambient atmosphere. Note that although there may be some differences in the

results based on different methods, the aging timescales obtained all represent the mixing and

aging rate of aerosol particles in the atmosphere, which affects aerosols atmospheric lifetime,

thus the environment and climate effects. As shown in Figure 7, the derived aging timescale

of aerosols in this study is comparable to the observational results reported in other urban

areas, such as Mexico City (3 hours; Moffet and Prather, 2009) and Los Angeles (3 hours;

431 Krasowsky et al., 2016). The result is also close to the aging timescale of particles in source

432 area of biomass burning in California (4 hours; Akagi et al., 2012). However, the aging time

433 of particles displays large spatial variations at different sites. For example, the aging

434 timescale of particles observed in Beijing (4.6 hours) was four times faster than that in

435 Houston (18 hours) where the precursors concentrations are extremely low (Peng et al., 2016).

436 ~~Overall~~Overall, the mixing/aging timescale of particles in Beijing achieved in this study is 5–

437 10 hours, which falls within the range of 2–10 hours in polluted areas obtained by other

438 studies. Therefore, our results are likely representative of the aging time scale of aerosols in

439 polluted urban areas. Furthermore, the aging time of particles obtained in ambient atmosphere

440 is much shorter than the default values adopted in most models, which is commonly with a

441 duration of 1.15–2.5 days. In addition, the values among different models range greatly from

442 1 to 20 days (Figure ~~8~~7). For example, a timescale of 20 days was used to represent a slow

443 aging process (i.e., coagulation) by Liu et al. (2011), as may be not properly applied in

444 regions with high particle number concentration where the particles coagulation is also

445 efficient (Chen et al., 2017).

446 Although using a dynamic parameterization scheme ~~of~~for particles aging in models

447 could achieve the application of different ~~particles~~ aging ~~time~~times to different regions, the

448 simulated values show large variations ~~and uncertainties~~ among different models. For

449 example, in RegCM4 model, the conversion time from fresh to aged BC ~~range~~ranges from

450 about 5 hours to 7 days (Ghosh et al., 2021). The range in the KAMM/DRAIS, however, is

451 only 2 hours to about 1.6 days (Riemer et al., 2004). ~~The~~Moreover, even in central-eastern

452 China, the aging ~~timescales~~timescale has been reported ~~ranging~~to range from 12 hours to 7

453 days ~~over central eastern China~~ based on a regional chemical transport model ~~by~~ (Chen et al~~.~~

454 ~~(.,~~ 2017), which is much longer than that derived in urban Beijing by this study. ~~–~~Additionally,

the aging times of carbonaceous aerosols simulated by the GEOS-Chem model exhibit large spatial and temporal variations, with the global average calculated to be 3.1 days (Huang et al., 2013). This value is much longer than the default values used in other global models (1-2 days) (Pierce et al., 2007). Note that although the mixing (aging) timescale of particles was determined by examining diurnal variations in the mixing state of aerosol particles in this study, compared with laboratory studies, various factors in the real ambient atmosphere change over time, including meteorological conditions, emission sources, and atmospheric processes etc. Therefore, the result derived in this study warrants further verifications. The long-term field measurements at more sites should be conducted in the future.

The large uncertainties in the aging timescale can significantly affect the accuracy of simulation and assessment for atmospheric lifetime, loading and radiation forcing of aerosols. For example, to better simulate the intercontinental transport of aerosols, Huang et al. (2013) implemented a variable aging scheme in the GEOS-Chem model, which showed that the total atmospheric burdens and global average lifetimes of BC (OC, organic carbon) were increase by 8% (2%) compared to the default value (1.15 days). Similarly, due to the implementation of the dynamic aging scheme in models, the column burden and surface mass concentration of carbonaceous aerosols increased during the dry season in the polluted Indo-Gangetic Plain, and the atmospheric heating increased by at least 1.2 W m^{-2} (Ghosh et al., 2021). Therefore, given the large spatiotemporal variations in aging timescale of particles, the study emphasizes the urgency of conducting investigations at more field sites. In addition, the other factors such as the meteorology, aerosol mass loading and particle sizes that affect the aerosols aging should be accounted for so as to improve the dynamic aging schemes in climate models.

477
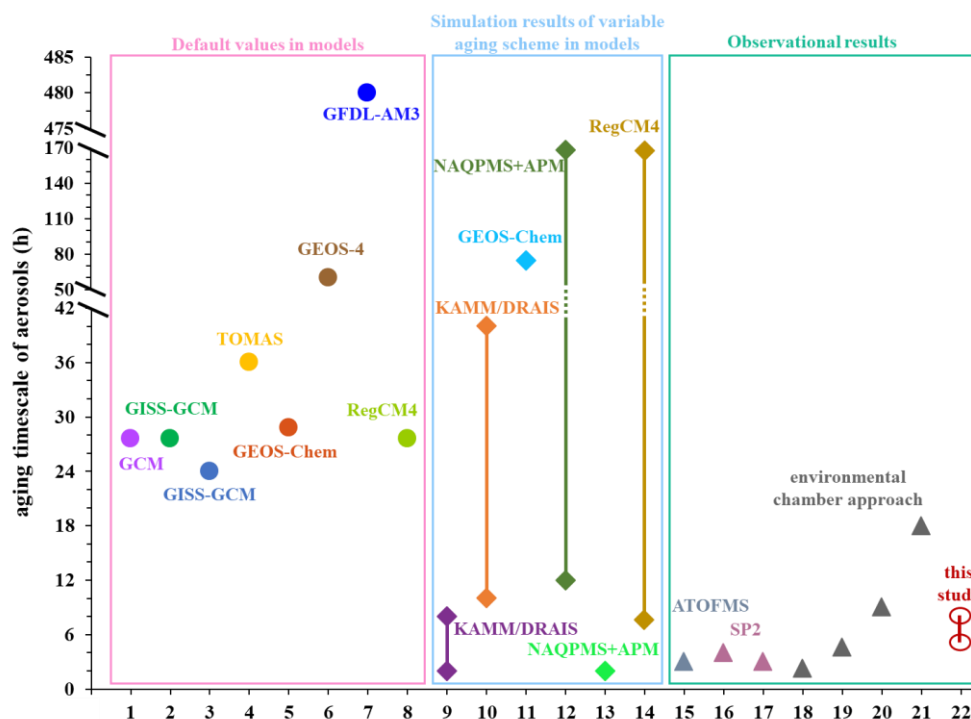
Figure ~~8~~7. The mixing/aging timescale of particles reported in literatures (1. Cooke et al.,

2002; 2. Chung and Seinfeld, 2002; 3. Koch and Hansen, 2005; 4. Pierce et al., 2007; 5. Yu

and Luo, 2009; 6. Colarco et al., 2010; 7. Liu et al., 2011; 8, 14. Ghosh et al., 2021; 9, 10.

Riemer et al., 2004; 11. Huang et al., 2013; 12, 13. Chen et al., 2017; 15. Moffet and Prather,

2009; 16. Akagi et al., 2012; 17. Krasowsky et al., 2016; 18-21. Peng et al., 2016). The solid

circle, diamond and the triangle denote the default aging time of particles used in models and

stimulation results of variable aging scheme in models, as well as the observational results,

respectively.

4 Conclusions

The real-time mixing state of ambient aerosol particles with dry particle sizes of 40, 80,

110, 150 and 200 nm was investigated in urban Beijing, according to PDF of hygroscopic

growth factor measured using the H-TDMA system. Four mixing states of ambient size-

resolved particles were captured in this study. In general, particles with LH ~~external, LH MH~~

491 ~~external~~internally-mixed, externally-mixed, transitional ~~external~~externally-mixed and ~~internal~~

492 ~~mixing~~MH internally-mixed state account for 0-10%,20-46%,17-24% and 27-56%

493 respectively, which depends on particles size greatly. The fraction of internally-mixed

494 particles peaks at 80 and 110 nm due to enhanced aging in intermediate particles. The diurnal

495 variation of mixing state of particles in all sizes considered ~~present~~presents a visible aging

496 process, showing that the fraction of particles with ~~internal mixing~~MH internally-mixed state

497 increases significantly from ~10-40% before 9:00 to about 100% during 12:00–15:00 on clear

498 days, accompanied by a growth in particle size from 20 nm to 100 nm~~, which is more notable~~

499 ~~than that on cloudy days. Specifically, the~~. Typically, the mixing/aging process of particles

500 ~~within~~takes approximately 5–~~8~~10 hours~~. In addition,~~, which reveals the mixing ~~state of~~

501 ~~particles was observed to be dependent both on T and RH, showing that~~(aging) timescale of

502 aerosols during the ~~particles with internal mixing state elevates obviously when T or RH~~

503 ~~exceeds 25°C or 60% respectively. Moreover, with the intensification of particulate pollution,~~

504 ~~the particles become more internally mixed. The~~campaign. Additionally, our results ~~indicate~~

505 ~~that both high ambient temperature and very humid atmosphere are more favorable for~~

506 ~~particle aging~~suggest that fine aerosol particles undergo significant aging through

507 photochemical processes in the polluted atmosphere~~. The~~ of urban Beijing. Furthermore, the

508 large difference of mixing/aging timescale of particles between values in models and the

509 timescale achieved by observations, emphasizing the vital role of exploring the aging

510 timescale through more field measurements to improve the accuracy of aging schemes in

511 climate models. The results revealed in our study highlight the considerable impact of

512 atmospheric aging on mixing state of fine aerosol particles in polluted megacities.

Data availability

All data used in the study are available from the corresponding author upon request (zhangfang2021@hit.edu.cn).

Author contributions

FZ and JL conceived the conceptual development of the paper. FZ directed and performed of the experiments with JR, LC and JL. JL conducted the data analysis and wrote the draft. All authors edited and commented on the various sections of the paper.

Competing interests

The authors declare that they have no conflict of interest.

Acknowledgments

This work was funded by the National Natural Science Foundation of China (NSFC) research project (Grant No. 42475112, 42405191), Shenzhen Science and Technology Plan Project (Grant No. GXWD20220811174022002; KCXST20221021111404011), Guangdong Natural Science Foundation (Grant No. 2024A1515011005), Hebei Natural Science Foundation (Grant No. D2024205006). We thank all participants in the field campaigns for their tireless work and cooperation.

Reference

Akagi, S. K., Craven, J. S., Taylor, J. W., McMeeking, G. R., Yokelson, R. J., Burling, I. R., Urbanski, S. P., Wold, C. E., Seinfeld, J. H., Coe, H., Alvarado, M. J., and Weise, D. R.: Evolution of trace gases and particles emitted by a chaparral fire in California.

535   Atmospheric Chemistry and Physics, 2012, , Atmos. Chem. Phys., 12(3),, 1397—1421.,

536   https://doi.org/10.5194/acp-12-1397-2012, 2012.

537   Chen X, Wang Z, Yu F, et al. Chen, L., Zhang, F., Yan, P., Wang, X., Sun, L., Li, Y., Zhang, X.,

538   Sun, Y., and Li, Z.: The large proportion of black carbon (BC)-containing aerosols in the

539   urban   atmosphere,   Environ.   Pollut.,   263,   Part   B,

540   https://doi.org/10.1016/j.envpol.2020.114507, 2020.

541   Chen, L., Zhang, F., Zhang, D., Wang, X., Song, W., Liu, J., Ren, J., Jiang, S., Li, X., and Li,

542   Z.: Measurement report: Hygroscopic growth of ambient fine particles measured at five

543   sites in China, Atmos. Chem. Phys., 22, 6773–6786, https://doi.org/10.5194/acp-22-

544   6773-2022, 2022.

545   Chen, X., Wang, Z., Yu, F., Pan, X., Li, J., Ge, B., Wang, Z., Hu, M., Yang, W., and Chen,

546   H.: Estimation of atmospheric aging time of black carbon particles in the polluted

547   atmosphere over central-eastern China using microphysical process analysis in regional

548   chemical transport model. Atmospheric Environment, 2017, 163, 44 56. , Atmos.

549   Environ., 163, 44–56, https://doi.org/10.1016/j.atmosenv.2017.05.016, 2017.

550   Chen L, Zhang F, Yan P, et al. The large proportion of black carbon (BC)-containing aerosols

551   in   the   urban   atmosphere.   Environmental   Pollution,   2020,   263,   114507.

552   https://doi.org/10.1016/j.envpol.2020.114507

553   Chen L, Zhang F, Zhang D, et al. Measurement report: Hygroscopic growth of ambient fine

554   particles measured at five sites in China. Atmospheric Chemistry and Physics, 2022, 22,

555   6773-6786.

556   Chung, S,., and Seinfeld, J.,.: Global distribution and climate forcing of carbonaceous aerosols.

Journal of Geophysical Research, 2002, J. Geophys. Res.-Atmos., 107(D19), 4407, doi:10.1029/2001JD001397https://doi.org/10.1029/2001JD001397, 2002.

Colarco, P., Silva, A., Chin, M, et al., and Diehl, T.: Online simulations of global aerosol distributions in the NASA GEOS-4 model and comparisons to satellite and ground-based aerosol optical depth. Journal of Geophysical Research, 2010, 115, D14207, doi:10.1029/2009JD012820, J. Geophys. Res.-Atmos., 115, D14207, https://doi.org/10.1029/2009JD012820, 2010.

Cooke, W., Ramaswamy, V., and Kasibhatla, P.: A general circulation model study of the global carbonaceous aerosol distribution. Journal of Geophysical Research: Atmospheres, 2002, J. Geophys. Res.-Atmos., 107(D16), 10.1029/2001JD001274https://doi.org/10.1029/2001JD001274, 2002.

Enroth, J., Mikkilä, J., Németh, Z, et al., Kulmala, M., and Salma, I.: Wintertime hygroscopicity and volatility of ambient urban aerosol particles. Atmospheric Chemistry and Physics, 2018, , Atmos. Chem. Phys., 18, 4533–4548, https://doi.org/10.5194/acp-18-4533-2018, 2018.

Fan, X., Liu, J., Zhang, F, et al., Chen, L., Collins, D., Xu, W., Jin, X., Ren, J., Wang, Y., Wu, H., Li, S., Sun, Y., and Li, Z.: Contrasting size-resolved hygroscopicity of fine particles derived by HTDMA and HR-ToF-AMS measurements between summer and winter in Beijing: Thethe impacts of aerosol aging and local emissions. Atmospheric Chemistry and Physics, 2020, , Atmos. Chem. Phys., 20(2), 915- 929, https://doi.org/10.5194/acp-20-915-2020, 2020.

Ge, S., Su, J., Zhao, P, et al., Li, J., Liu, S., Qiu, Y., Pu, W., and Ma, Z.: Characteristics of

579 PM2.5 hygroscopicity and the influences of water-soluble ions during haze events in

580 Beijing. Atmospheric Environment, 2024, 120382, Atmos. Environ., 120382,

581 https://doi.org/10.1016/j.atmosenv.2024.120382, 2024.

582 Ghosh, S., Riemer, N., Giuliani, G, et al., Giorgi, F., Ganguly, D., and Dey, S.: Sensitivity

583 of carbonaceous aerosol properties to the implementation of a dynamic aging

584 parameterization in the regional climate model RegCM. Journal of Geophysical

585 Research: Atmospheres, 2021, 126, e2020JD033613, J. Geophys. Res.-Atmos., 126,

586 https://doi.org/10.1029/2020JD033613, 2021.

587 Gysel, M., McFiggans GB, &, G. B., and Coe, H.: Inversion of tandem differential mobility

588 analyser (TDMA) measurements. Journal of, J. Aerosol Science, 2009, Sci., 40(2), 134

589 151., https://doi.org/10.1016/j.jaerosci.2008.07.013, 2009.

590 Hersey SP, S. P., Craven JS, J. S., Metcalf AR, et al., A. R., Lin, J., Lathem, T., Suski, K.,

591 Cahill, J., Duong, H., Sorooshian, A., Jonsson, H., Shiraiwa, M., Zuend, A., Nenes, A.,

592 Prather, K., Flagan, R., and Seinfeld, J.: Composition and hygroscopicity of the los

593 angeles aerosol: CalNex. Journal of Geophysical Research:Atmospheres, 2013, J.

594 Geophys. Res.-Atmos., 118(7): 3016-3036, https://doi.org/10.1002/jgrd.50307, 2013.

595 Hong J, Xu H, Tan H, et al.Hong, J., Xu, H., Tan, H., Yin, C., Hao, L., Li, F., Cai, M., Deng,

596 X., Wang, N., Su, H., Cheng, Y., Wang, L., Petäjä, T., and Kerminen, V.-M.: Mixing state

597 and particle hygroscopicity of organic-dominated aerosols over the Pearl River Delta

598 region in China. Atmospheric Chemistry and Physics, 2018, , Atmos. Chem. Phys., 18,

599 14079 14094, https://doi.org/10.5194/acp-18-14079-2018, 2018.

600 Hua, Y., Wang, S., Jiang, J., Zhou, W., Xu, Q., Li, X., Liu, B., Zhang, D., and Zheng, M.:

Characteristics and sources of aerosol pollution at a polluted rural site southwest in Beijing, China, Sci. Total Environ., 626, 519-527, https://doi.org/10.1016/j.scitotenv.2018.01.047, 2018.

Huang, Y., Wu, S., Dubey, M. K, et al., and French, N. H. F.: Impact of ageingaging mechanism on model simulated carbonaceous aerosols. Atmospheric Chemistry and Physics, 2013, , Atmos. Chem. Phys., 13, 6329–6343, https://doi.org/10.5194/acp-13-6329-2013, 2013.

Jacobson, M.: Strong radiative heating due to the mixing state of black carbon in atmospheric aerosols., Nature, 2001, 409(6821),, 695-697. 697, https://doi.org/10.1038/35055518, 2001.

Koch, D., Hansen, J.: Distant origins of Arctic black carbon: A Goddard Institute for Space Studies Model experiment. Journal of Geophysical Research, 2005,, J. Geophys. Res.-Atmos., 110, D04204, doi:10.1029/2004JD005296https://doi.org/10.1029/2004JD005296, 2005.

Krasowsky, T., McMeeking, G., Wang, D, et al., Sioutas, C., Ban-Weiss, G.: Measurements of the impact of atmospheric aging on physical and optical properties of ambient black carbon particles in Los Angeles. Atmospheric Environment, 2016,, Atmos. Environ., 142, 496-504, https://doi.org/10.1016/j.atmosenv.2016.08.010, 2016.

Liu, D., Joshi, R., Wang, J, et al., Yu, C., Allan, J. D., Coe, H., Flynn, M. J., Xie, C., Lee, J., Squires, F., Kotthaus, S., Grimmond, S., Ge, X., Sun, Y., and Fu, P.: Contrasting physical properties of black carbon in urban Beijing between winter and summer. Atmospheric Chemistry and Physics, 2019, , Atmos. Chem. Phys., 19, 6749–6769.,

623   https://doi.org/10.5194/acp-19-6749-2019, 2019.

624 Liu, J., Fan, S., Horowitz, L, ~~et al.~~, and Levy II, H.: Evaluation of factors controlling

625   long-range transport of black carbon to the Arctic. ~~Journal of Geophysical Research,~~

626   ~~2011,~~ J. Geophys. Res.-Atmos., 116, D04307, https://doi.org/10.1029/2010JD015145,

627   2011.

628 Liu, J., Zhang, F., Xu, W, ~~et al.~~, Sun, Y., Chen, L., Li, S., Ren, J., Hu, B., Wu, H., and

629   Zhang, R.: Hygroscopicity of organic aerosols linked to formation mechanisms.

630   ~~Geophysical Research Letters, 2021a,~~ Geophys. Res. Lett., 48, e2020GL091683,

631   https://doi.org/10.1029/2020GL091683, 2021a.

632 ~~Liu J, Zhang F, Xu W, et al.~~Liu, J., Zhang, F., Xu, W., Chen, L., Ren, J., Jiang, S., Sun, Y.,

633   and Li, Z.: A large impact of cooking organic aerosol (COA) on particle hygroscopicity

634   and CCN activity in urban atmosphere. ~~Journal of Geophysical Research: Atmospheres,~~

635   J. Geophys. Res.-Atmos., 126, e2020JD033628, https://doi.org/10.1029/2020JD033628,

636   2021b.

637 Li ~~W,~~, S., Zhang, F., Jin, X., Sun, Y., Wu, H., Xie, C., Chen, L., Liu, J., Wu, T., Jiang, S.,

638   Maureen, C., and Li, Z.: Characterizing the ratio of nitrate to sulfate in ambient fine

639   particles of urban Beijing during 2018–2019, Atmos. Environ., 237,

640   https://doi.org/10.1016/j.atmosenv.2020.117662, 2020.

641 Li, W., Sun, J., Xu ~~L, et al.~~, L., Shi, Z., Riemer, N., Sun, Y., Fu, P., Zhang, J., Lin, Y., Wang,

642   X., Shao, L., Chen, J., Zhang, X., Wang, Z., and Wang W.: A conceptual framework for

643   mixing structures in individual aerosol particles. ~~Journal of Geophysical Research:~~

644   ~~Atmospheres, 2016,~~ J. Geophys. Res.-Atmos., 121(22), 13784-13798,

645   https://doi.org/10.1002/2016JD025252, 2016.

646   Moffet, R~~.~~, and Prather, K~~.~~: In-situ measurements of the mixing state and optical properties

647   of soot with implications for radiative forcing estimates, ~~Proceedings of the National~~

648   ~~Academy of Sciences, 2009~~P. Natl. Acad. Sci. USA, 106(29), 11872-11877,

649   https://doi.org/10.1073/pnas.0900040106, 2009.

650   Müller, A~~.~~, Miyazaki, Y~~.~~, Aggarwal, S~~, et al.~~, Kitamori, Y., Boreddy, S., and Kawamura, K.:

651   Effects of chemical composition and mixing state on size-resolved hygroscopicity and

652   cloud condensation nuclei activity of submicron aerosols at a suburban site in northern

653   Japan in summer~~. Journal of Geophysical Research: Atmospheres, 2017,~~, J. Geophys.

654   Res.-Atmos., 122(17), 9301-9318, https://doi.org/10.1002/2017JD027286, 2017.

655   Peng, J~~.~~, F., Hu, M~~.~~, Guo, S~~, et al.~~, Du, Z. F., Zheng, J., Shang, D. J., Zamora, M., Zeng, L.

656   M., Shao, M., Wu, Y. S., Zheng, J., Wang, Y., Glen, C., Collins, D., Molina, M., and

657   Zhang, R. Y.: Markedly enhanced absorption, and direct radiative forcing of black

658   carbon under polluted urban environments~~. Proceedings of the National Academy of~~

659   ~~Sciences of the United States of America, 2016,~~ P. Natl. Acad. Sci. USA, 113~~(16),~~,

660   4266–4271~~.~~, https://doi.org/10.1073/pnas.1602310113, 2016.

661   Petters, M. D~~, &.~~ and Kreidenweis, S. M~~.~~: A single parameter representation of hygroscopic

662   growth and cloud condensation nucleus activity~~. Atmospheric Chemistry and Physics,~~

663   ~~2007,~~, Atmos. Chem. Phys., 7~~(8),~~, 1961–1971~~.~~,

664   https://doi.org/10.5194/acp-7-1961-2007, 2007.

665   Pierce, J~~.~~, R., Chen, K~~.~~, and Adams, P. J.: Contribution of primary carbonaceous aerosol to

666   cloud condensation nuclei: processes and uncertainties evaluated with a global aerosol

microphysics model. ~~Atmospheric Chemistry and Physics, 2007, 7, 7723-7765~~, Atmos. Chem. Phys., 7, 5447–5466, https://doi.org/10.5194/acp-7-5447-2007, 2007.

Pöschl, U., Letzel, T., Schauer, C~~, et al.~~, and Niessner, R.: Interaction of ozone and water vapor with spark discharge soot aerosol particles coated with benzo[a]pyrene : O_3 and H_2O adsorption, benzo[a]pyrene degradation, and atmospheric implications. ~~Journal of Physical Chemistry A~~, J. Phys. Chem. A, 16, 105, https://doi.org/10.1021/jp004137n, 2001.

Ren, J., Zhang, F., Wang, Y~~, et al.~~, Collins, D., Fan, X., Jin, X., Xu, W., Sun, Y., Cribb, M., and Li, Z.: Using different assumptions of aerosol mixing state and chemical composition to predict CCN concentrations based on field measurements in urban Beijing. ~~Atmospheric Chemistry and Physics, 2018,~~, Atmos. Chem. Phys., 18, 6907–6921, https://doi.org/10.5194/acp-18-6907-2018, 2018.

Ren, J., Zhang, F., Chen, L~~, et al.~~, Cao, G., Liu, M., Li, X., Wu, H., Cheng, Y., and Li, Z.: Identifying the hygroscopic properties of fine aerosol particles from diverse sources in urban atmosphere and the applicability in prediction of cloud nuclei. ~~Atmospheric Environment, 298,~~, Atmos. Environ., 298, 119615, https://doi.org/10.1016/j.atmosenv.2023.119615, 2023.

Riemer, N., Vogel, H., and Vogel, B.: Soot aging time scales in polluted regions during day and night. ~~Atmospheric Chemistry and Physics, 2004,~~, Atmos. Chem. Phys., 4 ~~(7)~~, 1885–1893, https://doi.org/10.5194/acp-4-1885-2004, 2004.

Riemer, N., Ault, A. P., West, M~~, et al.~~, Craig, R. L., and Curtis, J. H.: Aerosol mixing state: Measurements, modeling, and impacts. ~~Reviews of Geophysics, 2019,~~, Rev. Geophys.,

57, 187–249~~.~~, https://doi.org/10.1029/2018RG000615, 2019.

Saha, P. K~~.,.~~, Khlystov, A~~.,.~~, and Grieshop, A. P~~.:~~.: Downwind evolution of the volatility and mixing state of near-road aerosols near a US interstate ~~high way. Atmospheric Chemistry and Physics, 2018, 18(3): 2139-2154~~highway, Atmos. Chem. Phys., 18, 2139–2154, https://doi.org/10.5194/acp-18-2139-2018, 2018.

~~Shi J, Hong J, Ma N, et al.~~Shi, J., Hong, J., Ma, N., Luo, Q., He, Y., Xu, H., Tan, H., Wang, Q., Tao, J., Zhou, Y., Han, S., Peng, L., Xie, L., Zhou, G., Xu, W., Sun, Y., Cheng, Y., and Su, H.: Measurement report: On the difference in aerosol hygroscopicity between high and low relative humidity conditions in the North China Plain~~. Atmospheric Chemistry and Physics, 2022,~~, Atmos. Chem. Phys., 22, 4599–4613, https://doi.org/10.5194/acp-22-4599-2022, 2022.

Spitieri, C~~.,.~~, Gini, M~~.,.~~, Gysel-Beer, M~~, et al.~~, and Eleftheriadis, K.: Annual cycle of hygroscopic properties and mixing state of the suburban aerosol in Athens, Greece~~.~~, Atmos. Chem. Phys., 23, 235-249, https://doi.org/10.5194/acp-23-235-2023, 2023.

Stevens, R., and Dastoor, A.: A Review of the Representation of Aerosol Mixing State in Atmospheric ~~Chemistry and Physics, 2023, 23, 235-249~~Models, Atmos., 10(4), 168, https://doi.org/10.3390/atmos10040168, 2019.

~~Swietlicki E, Hansson H C, Hameri K, et al.~~Sun, Y. L., Wang, Z. F., Du, W., Zhang, Q., Wang, Q. Q., Fu, P. Q., Pan, X. L., Li, J., Jayne, J., and Worsnop, D. R.: Longterm real-time measurements of aerosol particle composition in Beijing, China: seasonal variations, meteorological effects, and source analysis, Atmos. Chem. Phys., 15, 10149–10165, https://doi.org/10.5194/acp-15-10149-2015, 2015.

Swietlicki, E., Hansson, H. C., Hameri, K., Svenningsson, B., Massling, A., Mcfiggans, G., P. Mcmurry, H., Petäjä, T., Tunved, P., Gysel, M., Topping, D., Weingartner, E., Baltensperger, U., Rissler, J., Wiedensohler, A., and Kulmala, M.: Hygroscopic properties of submicrometer atmospheric aerosol particles measured with H-TDMA instruments in various environments - a review. ~~Tellus B, 2008, 60, 432 469. ~~, Tellus B, 60(3), 432–469, https://doi.org/10.1111/j.1600-0889.2008.00350.x, 2008.

~~Wang Q, Huang R J, Cao J, et al. Mixing State of Black Carbon Aerosol in a Heavily Polluted Urban Area of China: Implications for Light Absorption Enhancement. Aerosol Science and Technology, 2014, 48:7, 689 697.~~

~~Wang Y, Li Z, Zhang R, et al.~~Wang, Y., Li, Z., Zhang, R., Jin, X., Xu, W., Fan, X., Wu, H., Zhang, F., Sun, Y., and Wang, Q.: Distinct ultrafine- and accumulation-mode particle properties in clean and polluted urban environments~~. Geophysical Research Letters, 2019, 46, 10,918 10,925~~, Geophys. Res. Lett., 46, 10,918–10,925, https://doi.org/10.1029/2019GL084047, 2019.

Wang~~,~~ Y~~.,~~, Ma~~,~~ P~~.,~~-L., Peng~~,~~ J~~, et al.~~., Zhang, R., Jiang, J. H., Easter, R. C., and Yung, Y. L.: Constraining ~~ageing~~aging processes of black carbon in the ~~community atmosphere model~~Community Atmosphere Model using environmental chamber measurements~~.~~ ~~Journal of Advances in Modeling~~, J. Adv. Model. Earth ~~Systems, 2018,~~Sy., 10, 2514–2526. https://doi.org/10.1029/2018MS001387, 2018.

~~Wu Z J, Zheng J, Shang D J, et al. Particle hygroscopicity and its link to chemical composition in the urban atmosphere of Beijing, China, during summertime. Atmospheric Chemistry and Physics, 2016, 16(2), 1123 1138.~~

Xu W, Chen C, Qiu Y, et al. Wang, Z., Shi, C., Zhang, H., Chen, Y., Chi, X., Xia, C., Wang, S., Zhu, Y., Zhang, K., Chen, X., Xing, C., and Liu, C.: Measurement report: Dust and anthropogenic aerosols' vertical distributions over northern China dense aerosols gathered at the top of the mixing layer, Atmos. Chem. Phys., 23, 14271–14292, https://doi.org/10.5194/acp-23-14271-2023, 2023.

Winkler, P.: The growth of atmospheric aerosol particles as a function of the relative humidity—II. An improved concept of mixed nuclei, J. Aerosol Sci., 4(5), 373–387, https://doi.org/10.1016/0021-8502(73)90027-X, 1973.

Xie, C., He, Y., Lei, L., Zhou, W., Liu, J., Wang, Q., Xu, W., Qiu, Y., Zhao, J., Sun, J., Li, L., Li, M., Zhou, Z., Fu, P., Wang, Z., and Sun, Y.: Contrasting mixing state of black carbon-containing particles in summer and winter in Beijing, Environ. Pollut., 263, 114455, https://doi.org/10.1016/j.envpol.2020.114455, 2020.

Xu, W., Chen, C., Qiu, Y., Xie, C., Chen, Y., Ma, N., Xu, W., Fu, P., Wang, Z., and Pan, X.: Size-resolved characterization of organic aerosol in the North China Plain: new insights from high resolution spectral analysis. Environmental Science: Atmospheres, 2021, 1(6), 346–358, Environ. Sci.: Atmos., 1(6), 346–358, https://doi.org/10.1039/D1EA00025J, 2021.

Xie C, He Y, Lei L, et al. Contrasting mixing state of black carbon containing particles in summer and winter in Beijing. Environmental Pollution, 2020, 263, 114455.

Xu, W., Xie, C., Karnezi, E., Zhang, Q., Wang, J., Pandis, S. N., Ge, X., Zhang, J., An, J., Wang, Q., Zhao, J., Du, W., Qiu, Y., Zhou, W., He, Y., Li, Y., Li, J., Fu, P., Wang, Z., Worsnop, D. R., and Sun, Y.: Summertime aerosol volatility measurements in Beijing,

China, Atmos. Chem. Phys., 19, 10205–10216, https://doi.org/10.5194/acp-19-10205-2019, 2019.

Yao, Y., Curtis, J. H., Ching J, et al., J., Zheng, Z., and Riemer, N.: Quantifying the effects of mixing state on aerosol optical properties. Atmospheric Chemistry and Physics, 2022,, Atmos. Chem. Phys., 22, 9265—9282, https://doi.org/10.5194/acp-22-9265-2022, 2022.

Yu, F., and Luo, G.: Simulation of particle size distribution with a global aerosol model: contribution of nucleation to aerosol and CCN number concentrations. Atmospheric Chemistry and Physics, 2007, 9, 10597-10645, Atmos. Chem. Phys., 9, 7691–7710, https://doi.org/10.5194/acp-9-7691-2009, 2009.

Zhang S, Shen X, Sun J, et al. Atmospheric Particle Hygroscopicity and the Influence by Oxidation State of Organic Aerosols in Urban Beijing. Journal of Environmental Sciences, 2023, 124, 544-556.

Zhang, F., Wang, Y., Peng, J., Ren, J, et al.., Collins, D., Zhang, R., Sun, Y., Yang, X., and Li, Z.: Uncertainty in Predicting CCN Activity of Aged and Primary Aerosols. Journal of Geophysical Research: Atmospheres, 2017,, J. Geophys. Res.-Atmos., 122, 11723–11736., https://doi.org/10.1002/2017JD027058, 2017.

Zhang J, Liu, J, Tao S, et al. Long-range transport of black carbon to the Pacific Ocean and its dependence on aging timescale, Atmospheric Chemistry and Physics, 2015, 15(20), 11521-11535.

Zhang J,, Li, W,. Wang Y, et al., Y., Teng, X., Zhang, Y., Xu, L., Yuan, Q., Wu, G., Niu, H., and Shao, L.: Structural collapse and coating composition changes of soot particles

777   during long-range transport. ~~Journal of Geophysical Research: Atmospheres, 2023,~~ J.

778   Geophys. Res.-Atmos., 128, e2023JD038871~~.~~

779   ~~Zhang Y, Liu H, Lei S, et al. Mixing state of refractory black carbon in fog and haze at rural~~

780   ~~sites in winter on the North China Plain. Atmospheric Chemistry and Physics, 2021, 21,~~

781   ~~17631 17648.~~, https://doi.org/10.1029/2023JD038871, 2023.